

Streaking of a Picosecond Electron Pulse with a Weak Terahertz Pulse

Wataru Yajima, Yusuke Arashida,* Ryota Nishimori, Yuga Emoto, Yuki Yamamoto, Kohei Kawasaki, Yuri Saida, Samuel Jeong, Keishi Akada, Kou Takubo, Hidemi Shigekawa, Jun-ichi Fujita, Shin-ya Koshihara, Shoji Yoshida, and Masaki Hada*



Cite This: *ACS Photonics* 2023, 10, 116–124



Read Online

ACCESS |



Metrics & More



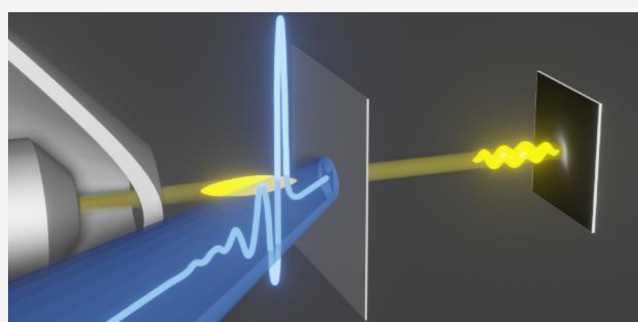
Article Recommendations



Supporting Information

ABSTRACT: Optoelectronic devices driven by terahertz (THz) waves have been used to control electron pulses, such as through acceleration, compression, and characterization of ultrashort pulsed electrons. In this study, we developed a THz generation setup with a lithium niobate crystal via the tilted-pump-pulse-front approach. Furthermore, a THz electro-optical sampling setup, an ultrashort pulsed electron generation system, and a THz streaking system with a simple butterfly-shaped THz optoelectronic resonator were also developed to determine the lower limits of THz intensities that can be used for characterization of picosecond pulsed electrons. Multiple deflections of the electron pulse occur when the duration is longer than the half cycle of the electric field at the THz optoelectronic resonator, which requires a higher THz intensity and makes the analyses difficult. The results obtained with appropriate analyses show that a weak THz field of a few kV/cm resonated with the THz optoelectronic device is sufficient to characterize picosecond pulsed electrons.

KEYWORDS: terahertz wave, electron beam, streaking method, pulse duration characterization, ultrafast time-resolved electron diffraction, ultrafast phenomena



INTRODUCTION

Ultrafast time-resolved electron diffraction measurements have directly provided the atomic-level structural dynamics of molecules or materials rearranged by photoexcitation on the femto-to-picosecond time scale.^{1–14} The time resolution of ultrafast time-resolved electron diffraction measurements relies on the pulse duration of the probe electron pulse since the optical pulse used for excitation (approximately 100 fs) is usually shorter than the electron pulse. Thus, the characterization of the probe electron pulse is essential. The interactions of electric fields and electrons have been used to measure the duration of electron pulses, that is, the interactions of laser-plasma with electron pulses (plasma method),^{15–19} the interactions of ponderomotive forces with electron pulses (ponderomotive method),^{20–24} the interactions of the instantaneous high voltage electric fields and electron pulses (photoswitch streaking method),^{25–27} and the interactions of electric fields generated by terahertz (THz) waves and electron pulses (THz streaking method).^{28–33} The fast response form sample is also used to estimate the pulse duration.^{34–36} The plasma method constructs a relatively simple setup compared with other methods; however, the accuracy of the pulse duration is limited since the laser plasma occurs on the picosecond time scale. The ponderomotive

method requires a specific optical setup inside the vacuum chamber. The photoswitch streaking method involves fabricating an ultrafast photoswitching device based on low-temperature grown GaAs substrates. THz generation, and characterization systems outside the vacuum chamber are required for the THz streaking method. Among these techniques, the THz streaking method would be one of the suitable options for the already existing ultrafast time-resolved electron diffraction setups because very large reconstruction inside the vacuum chamber is not required for this method.^{29–33} THz streaking techniques that are applied for electron pulses or X-ray free electron lasers have been reported in several studies.^{37–41} THz waves can also be used to control the acceleration, deflection, and compression of electron pulses.^{29,32} However, most studies on the THz streaking of electron pulses used experimental setups that

Received: August 22, 2022

Published: December 13, 2022



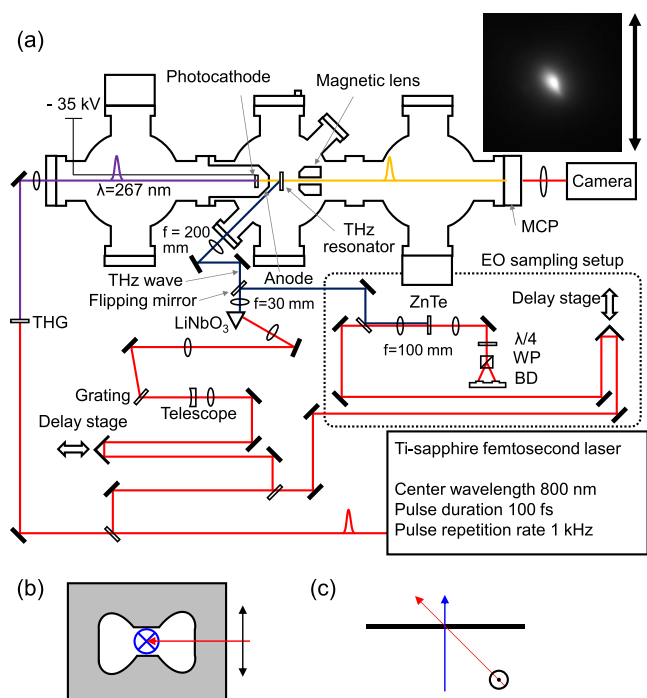


Figure 1. (a) Schematic of the electron beam pulse duration measurement setup by the THz streaking method. The electron beam shape at the CMOS camera is inset in the figure. The black arrow in the inset indicates the deflection direction of the electron beam by the THz pulse. The symbols THG, MCP, WP, and BD correspond to the third harmonic generation, microchannel plate, Wollaston prism, and balanced photodetector, respectively. Front view (b) and top view (c) of the orientation of the butterfly shape, the direction of electron beam propagation (blue arrows), the direction of THz wave propagation (red arrows), and the polarization axis of the THz wave (black arrows).

were customized to maximize the interaction of THz waves and electron pulses through THz streaking. Therefore, whether very weak THz can be utilized for the THz streaking method is worth determining. This method also has considerable merit for the already existing ultrafast time-resolved electron diffraction setups because of space limitations. In an existing setup, the THz beam may be interfered with by the sample holder or magnetic lens. In addition, the THz focusing optics may not always be placed

very close to the THz resonating device, leading to beam diameter enlargement at the THz optoelectronic resonating device. In this study, we developed a THz generation setup with a lithium niobate (LiNbO₃) crystal, a THz electro-optical (EO) sampling setup, an ultrashort pulsed electron generation system, and a THz streaking system with a simple butterfly shaped optoelectronic device to determine the lower limits of THz intensities that can be used for characterization of picosecond pulsed electrons. The fundamental principle of the butterfly shaped THz resonator is similar to the field enhancement effects of ultraviolet, visible, or infrared light at the metal nanostructures used in photon-induced near-field electron microscopy experiments.⁴² Another challenge involves the characterization of picosecond pulsed electrons with the THz streaking method. When the electron pulse is shorter than the half period of the main component of the electric field generated at the THz resonator, we cannot directly measure the duration of the electron pulse by the width broadening of the electron spot (streaking length) because such an electron beam is deflected more than once, i.e., undergoes multiple deflections. Due to the multiple deflections, the THz streaking signals with high frequency and high intensity are overlapped at the same position on the screen. Therefore, the streaking signals with low frequency and low intensity are obtained. Thus, it requires a relatively higher THz intensity when multiple deflections occur. In this situation, the electron pulse duration cannot be determined simply by the streaking length on the screen. We analyzed the obtained THz streaking signals with low frequency and low intensity and showed that a weak (a few kV/cm) THz field resonated with the optoelectronic device is sufficient to characterize femto-to-picosecond pulsed electron.

EXPERIMENTAL METHODS

A THz generation setup, EO sampling setup, ultrashort pulsed electron generation system, and THz streaking system are shown in Figure 1a. An optical pulse from a Ti:sapphire regenerative amplifier with a wavelength of 800 nm, a pulse duration of 100 fs, and a repetition rate of 1 kHz was split into two arms (electron generation arm and THz generation arms) with a beam splitter. An optical pulse in the electron generation arm was converted into an ultraviolet (UV) pulse at a wavelength of 267 nm with nonlinear optical crystals via third harmonic generation. The UV pulse was focused onto

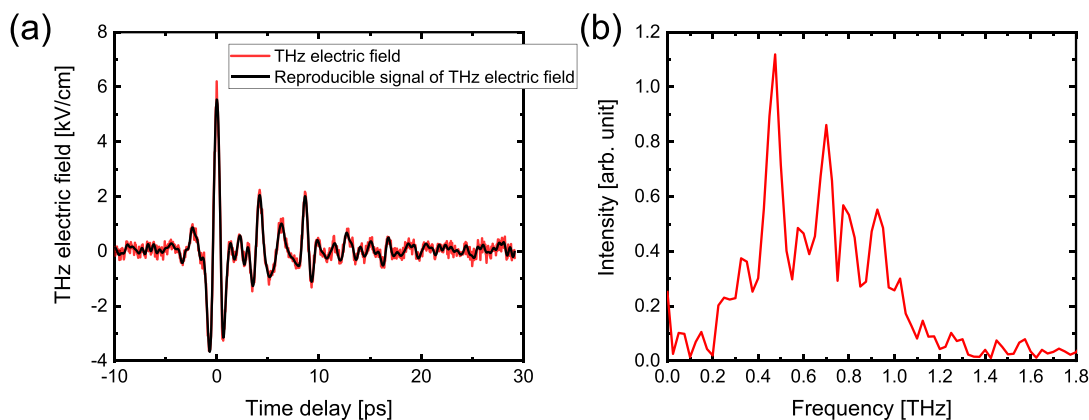


Figure 2. (a) Waveform of the THz pulse obtained by EO sampling and (b) its Fourier transform (intensity spectrum). The black line indicates the reproducible signal.

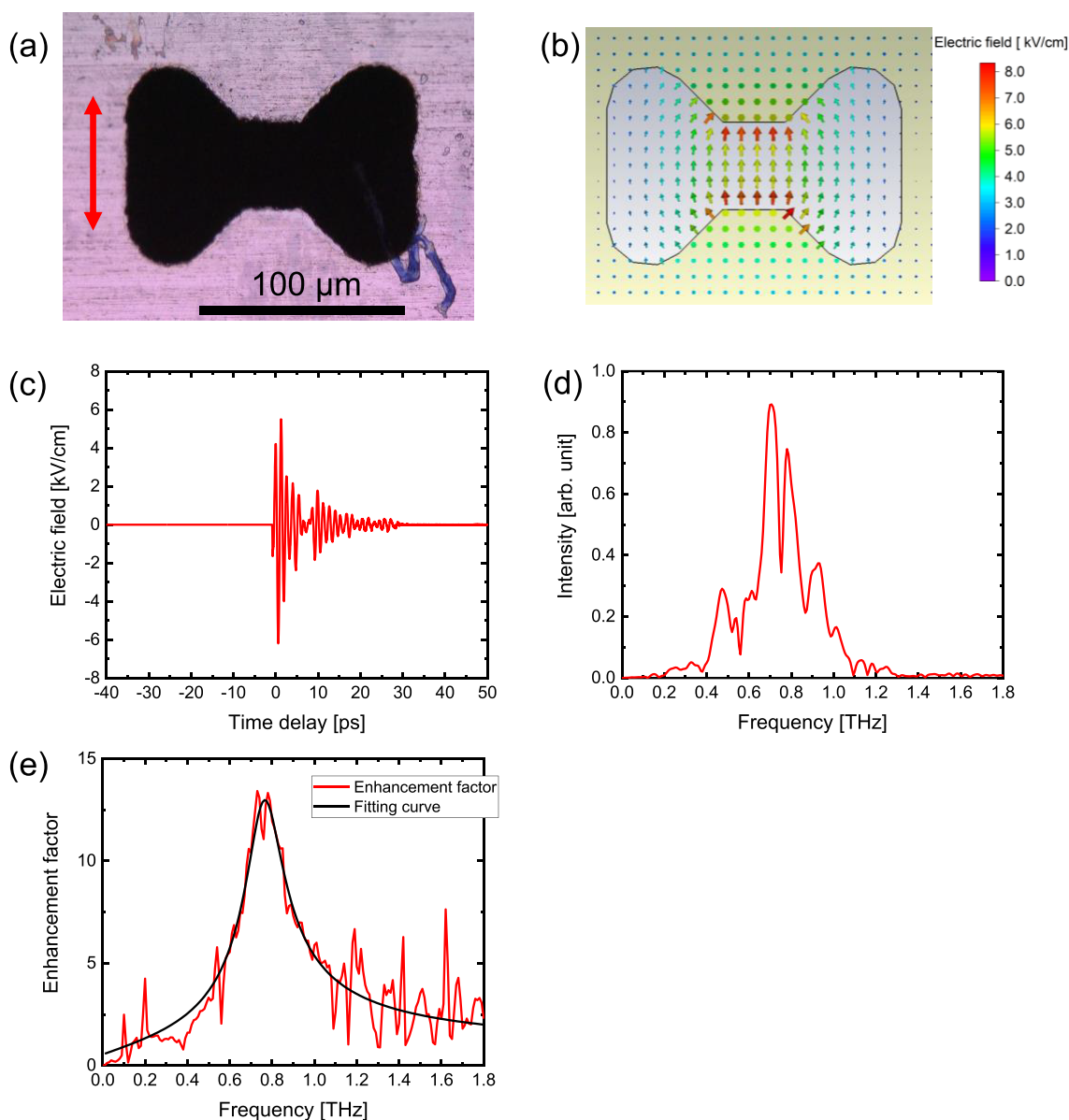


Figure 3. (a) Photograph of the THz optoelectronic resonator. The THz pulse has a polarization angle at which the electric field oscillates, as indicated by the red arrow. (b) Two-dimensional map of the calculated electric field distribution generated by the THz pulse at the THz optoelectronic resonator shown in a vectorial manner. The simulations are performed to set the electric field component of the THz optoelectronic resonator parallel to the polarization angle of the incident THz pulse. (c) Simulated waveform of the absolute value of the electric field generated in the central part of the THz optoelectronic resonator and (d) its Fourier transform (intensity spectrum). (e) Local field enhancement as a function of the frequency.

the Au photocathode to generate an electron pulse in a vacuum chamber of the ultrashort pulsed electron generation system. A 35 kV electrostatic field accelerated an electron pulse generated by the photoelectric effect. A pinhole resized the electron beam to 100 μm in diameter, which is slightly smaller than the clear aperture of the THz optoelectronic resonator. The typical duration of an electron pulse generated from a direct-current electron gun is a few ps. After passing through the THz optoelectronic resonator, the electron pulse was focused with a magnetic lens, hit on a microchannel plate, and detected by a complementary metal oxide semiconductor (CMOS) camera. The electron beam on the CMOS camera is shown in the inset of Figure 1a. The geometry of the orientation of the butterfly shape, the direction of electron beam propagation, the direction of THz wave propagation,

and the polarization axis of the THz wave are shown in Figure 1b,c.

We chose a tilted-pump-pulse-front scheme with a LiNbO₃ crystal to generate the THz pulse.^{43–45} Since the initial diameter of the optical pulse was 12 mm, which is large for the following optical systems, the optical pulse, after passing through a delay stage, was reduced in diameter to 6 mm using a telescope. The pulse front of the optical pulse was tilted using a transmission grating to match the THz generation angle at the LiNbO₃ crystal, with a focusing diameter of ~ 1 mm. A THz optical pulse with a source diameter of ~ 1 mm was generated from a LiNbO₃ crystal. The first lens with a focal length of 30 mm parallelized the diverged THz wave generated from a LiNbO₃ crystal. The size of the parallel THz beam was measured to be ~ 15 mm. The parallel THz wave

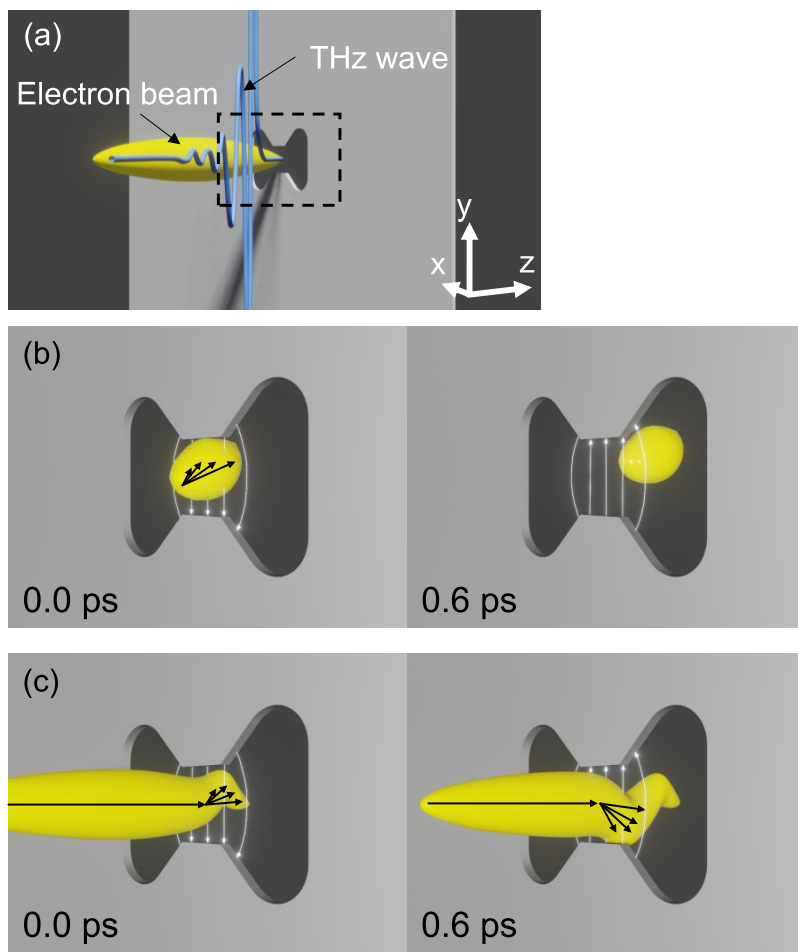


Figure 4. (a) Zoomed-out schematic illustration depicting the THz resonator with the electron beam and THz wave. An *xyz*-axis indicator is the inset in the figure. Zoomed-in schematic illustrations of the multiple deflections of short (b) and long (c) electron pulses. The yellow ellipsoid shows the electron pulse. The solid white and black arrows are the electric field and the direction of the electron pulse, respectively.

was focused on the THz optoelectronic resonator by the second lens with a focal length of 200 mm. The beam size on the THz resonator was ~ 7 mm based on the ratio of the focal lengths of the two lenses. The electron pulse streaked by the THz pulse was observed by changing the time delay between the electron pulse and THz pulse reaching the resonator with the delay stage. According to the calculation of the camera length, the one-pixel shift of the electron pulse on the CMOS camera corresponds to an electron deflection of $75 \mu\text{rad}$. To obtain a temporal profile of the THz electric field, we developed an EO sampling setup with a ZnTe crystal. For EO sampling, we used a fundamental optical pulse for the probe. A flipping mirror can switch the THz pulse to introduce it to either the electron streaking system or EO sampling setup.

RESULTS AND DISCUSSION

The THz optical pulse was characterized by EO sampling measurements with a near-infrared probe light. Figure 2a,b show a temporal profile of the THz wave measured from EO sampling measurements and its Fourier transform spectrum, respectively. The results show that the THz pulse has a frequency from 0.3–1.0 THz. The typical THz frequency generated from the LiNbO₃ crystal is 0–3 THz,⁴⁴ and we determined that the oscillation with a frequency from 0–3 THz was a reproducible signal. The THz electric field was

calculated to be 6.2 kV/cm at the EO sampling setup using the following equation:⁴⁶

$$E_T \cong \frac{c}{\omega n^3 r_{41} d} \frac{\Delta I}{I_0} \quad (1)$$

where E_T , c , ω , n , d , ΔI , and I_0 are the electric field of the THz wave, speed of light, angular frequency of the probe light, refractive index of the nonlinear optical crystal (ZnTe) for the probe light, thickness of the nonlinear optical crystal (ZnTe), modulated intensity of the probe light, and initial intensity of the probe light, respectively. A pyroelectric detector also measured the intensity of the THz pulse. The generated THz pulse at the LiNbO₃ crystal was estimated to be approximately 100 kV/cm; however, beam defocusing by lenses, reflection loss by mirrors, and absorption by air decrease the intensity of the THz pulse at the position of the EO sampling setup and the THz optoelectronic resonator. The THz pulse was generated from a point source (diameter of ~ 1 mm) as a spherical wave; therefore, we placed a lens with a short focal length ($f = 30$ mm) just behind the LiNbO₃ crystal to transform the wave into a parallel wave. In the EO sampling setup, another lens ($f = 100$ mm) was set to obtain a large incident fluence at the surface of the ZnTe crystal. The diameter of the THz optical beam was defined by the ratio of the focal lengths of the two lenses because the diameter of the THz beam at the LiNbO₃ crystal had a finite size. The focal

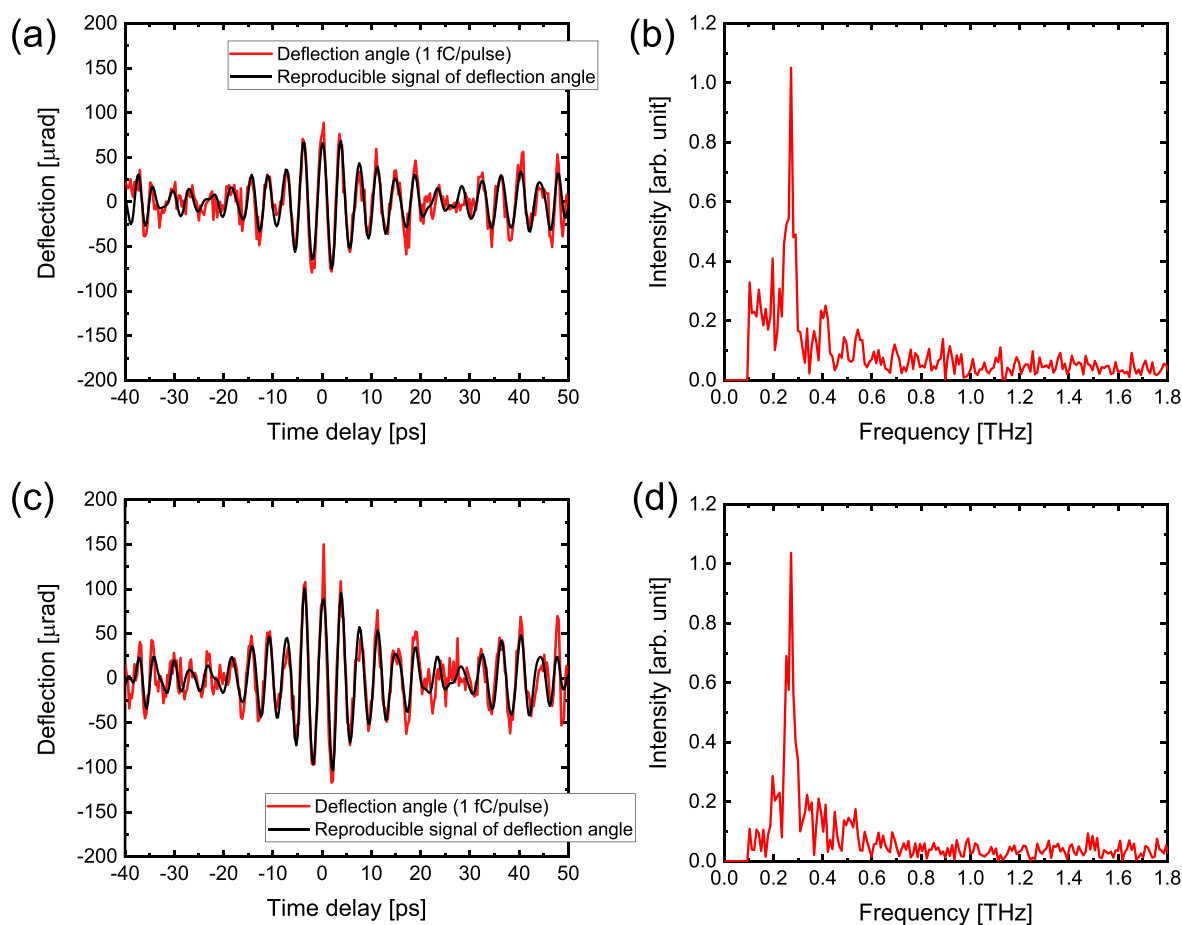


Figure 5. (a) Degree of deflection of the electron beam (1 fC/pulse) by the electrical field at the THz optoelectronic resonator as a function of the delay time and (b) its Fourier transform (intensity spectrum). (c) Deflection of the electron beam (2 fC/pulse) and (d) its Fourier transform (intensity spectrum). The following discussion shows that higher frequencies (>0.5 THz) are considered noise because the convolution with the electron pulse should attenuate the higher frequency signal. Lower frequencies (<0.1 THz) are also considered noise because of the stability of beam pointing. The oscillation with a frequency from 0.1–0.5 THz is determined to be a reproducible signal. The black lines indicate the reproducible signals in (a) and (c).

length of the lens for focusing on the THz optoelectronic resonator was 200 mm due to space limitations. Since the large beam (~ 15 mm) was gradually focused on the THz resonator (~ 7 mm), half of the THz beam was interfered with by the anode in this setup. The THz electric field at the THz optoelectronic resonator was estimated to be 2.6 kV/cm at the maximum.

An aluminum film thickness of 30 μm was used as a THz optoelectronic resonator. Figure 3a shows the resonator mechanically processed in a butterfly shape. The direction of the THz electric field is depicted as arrows inset in the picture. Using the results of EO sampling, an electric field in the THz optoelectronic resonator induced by the THz optical pulse was calculated by the finite difference time domain method in CST Studio Suite (Dassault Systèmes). Figure 3b shows the two-dimensional distribution of the electric field intensity at $t = 0$ from the calculation. The electric field was amplified at the center of the butterfly shape. The three-dimensional electric field of the profile of the THz resonator at $t = 0$ is shown in Figure S1. Since we used an *s*-polarized THz wave, the effects of the *x*- and *z*-axes are negligibly small, as shown in the three-dimensional simulated electric field at the resonator. Thus, the phase modulation effect of the THz wave interfered with by the resonator would be small in the

present case.⁴⁷ A temporal profile of the THz wave at the center of the THz optoelectronic resonator obtained by the calculation and its Fourier transform spectrum are shown in Figure 3c and d, respectively. According to the simulation, the electric field at the center of the resonator contains frequency components of 0.2–1.1 THz. Figure 3e shows the local field enhancement (Fourier spectrum of $E_{\text{out}}/E_{\text{in}}$) as a function of the frequency. The maximum local field enhancement is approximately 13 at the frequency of ~ 0.75 THz. For the present THz streaking measurements, the local field enhancement at frequencies of 0.27–0.41 THz is more critical, and the value at frequencies of 0.27–0.41 THz is 1.7–3.1. The electric field enhancement by the THz resonator is well described by the simple RLC model, as shown in the Supporting Information, Figure S2.

The duration of the electron pulse can be measured by the streak length on the screen when the electron pulse is shorter than the half cycle of the electric field generated by the THz wave (Figure 4a), where the half cycle of the electric field corresponds to ~ 0.6 ps. However, as shown in Figure 4b, multiple deflections occur for an electron pulse that is longer than the half cycle of the electric field generated by the THz wave; that is, when the electron pulse duration is longer than the half cycle of the THz streaking field, the electron pulse is

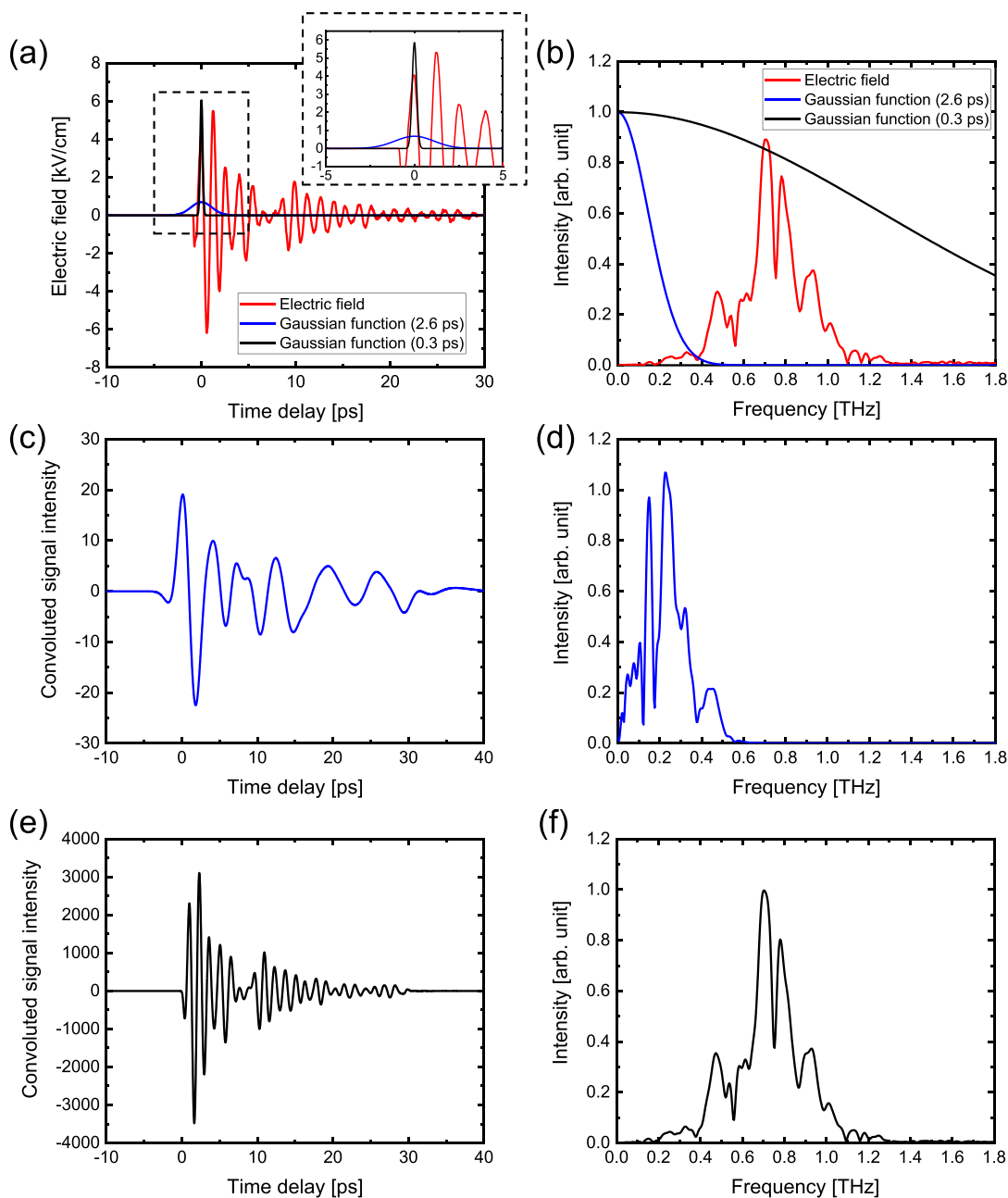


Figure 6. (a) Simulated waveform of the electric field generated in the central part of the THz optoelectronic resonator and the Gaussian functions (half-widths of 0.3 and 2.6 ps) representing the electron beam pulse distribution. The inset is an enlarged view of the black dashed area. (b) Fourier transform (intensity spectra) of the waveform of the electric field and the Gaussian functions shown in (a). (c) Calculated waveform of the electric field convolved with the extended Gaussian function (2.6 ps) and (d) its Fourier transform (intensity spectrum). (e) Calculated waveform of the electric field convolved with the short Gaussian function (0.3 ps) and (f) its Fourier transform (intensity spectrum).

deflected several times at the resonator. Therefore, the duration of the electron pulse cannot be estimated only by the streak length. In this case, the signal from the fast deflection is deformed, and the slow components are recorded on the screen.

Figure 5a,b shows the time-dependent electron deflection, derived from the center position of the electron, by the THz wave and its Fourier transform spectrum, where the electron pulse contains a charge of 1 fC. Similarly, those results with an electron pulse containing a charge of 2 fC are shown in Figure 5c,d. As shown in Figure 5a, the degree of electron deflection vibrated depending on the time delay. The Fourier transform spectrum of the electron deflection (Figure 5b) is different

from that of the electric field at the THz optoelectronic resonator (Figure 3d). This discrepancy occurs because the electron pulse duration is longer than the rise time of the electric field generated at the resonator and because of the aforementioned multiple-deflection effect.

The temporal profile of the electron deflection should correspond to the convolution of the electron pulse and electric field to consider the multiple deflections (Figure 6a) as follows:

$$h(t) = \int_{-\infty}^{\infty} f(t - \tau)g(\tau)d\tau \quad (2)$$

where $h(t)$, $f(t)$, and $g(t)$ are the temporal profiles of the electron deflection, the electric field at the THz optoelectronic resonator, and the electron pulse (Gaussian function), respectively. In the Fourier space, this convolution is reduced to simple multiplication, as shown in the following equation:

$$H(\omega) = F(\omega)G(\omega) \quad (3)$$

where $H(\omega)$, $F(\omega)$, and $G(\omega)$ are the Fourier transforms of $h(t)$, $f(t)$, and $g(t)$, respectively. A temporal profile of the electron pulse and its Fourier components used for the convolution are shown as the blue (longer electron pulse) and black (shorter electron pulse) lines in Figure 6a,b. An electron pulse was set as a Gaussian function with a pulse duration of 2.6 ps. The calculated time profile of the convolution of the electron pulse and electric field at the THz optoelectronic resonator and its Fourier transform spectrum are shown in Figure 6c and d, respectively. Lower frequency components were emphasized, and higher frequency components were suppressed. The convolution with a Gaussian function works as a low-pass filter, as shown in Figure 6b. The time profiles of the electron pulse deflection from both the experiment and the simulation had peaks at 0.27 and 0.42 THz. Compared with the experimental signal for the calculation, the half-width of the electron pulse was estimated to be 2.6 ps. We define $t = 0$ as the peak of the envelope of the electron deflection. The Hilbert transform provides the electron deflection envelope, as shown in the Supporting Information (Figure S3). According to the Hilbert transform, the accuracy of $t = 0$ is estimated to be ~ 90 fs (rms), which is comparable to the value (~ 50 fs rms) obtained for the XFEL with timing jitter correction.³⁶ The Fourier transform spectra obtained by the experiment and calculation agree well with each other (Figure 5b and Figure 6d). However, the experimental waveform (Figure 5a) is not reproduced in the calculation (Figure 6c). Note that the electron pulse is larger (100 μm in diameter) than the aperture of the THz optoelectronic resonator (50 $\mu\text{m} \times 50 \mu\text{m}$), and thus, the electric field applied to the electron beam in the resonator is not uniform in the experiment. We calculated the electron deflection at several points in the resonator (Supporting Information), and the average of these electron deflections (Figure S4) is almost the same as the waveform at the center part shown in Figure 6c. The Supporting Information shows that the difference between the experimental and calculated waveforms is caused by the deflection of the electron pulse by the original THz wave (Figure S5). From the 2 fC/pulse results, the peak of 0.42 THz was decreased compared with 1 fC/pulse. This suggests that the increase in the electron pulse duration, that is, the duration of the electron pulse with 2 fC/pulse, would be more than 3 ps. Thus, the extremely weak THz field of less than a few kV/cm resonated with the optoelectronic device is sufficient to characterize the picosecond electron pulse duration. Because multiple deflections would not occur in a shorter electron pulse (<0.6 ps), the required THz intensity would be estimated to be even smaller than kV/cm. Owing to the suppression of the multiple deflections, the intensity of the convoluted signal of the electric field generated at the THz resonator and shorter Gaussian function is much stronger than that with the more extended Gaussian function (Figure 6e,f). Thus, the electric field at the THz resonator will more effectively work for the shorter electron pulse. The duration of an electron pulse that is shorter than 0.6 ps will be more easily detected using this THz streaking system.

CONCLUSION

In summary, we developed a THz generation setup with a LiNbO₃ crystal, a THz EO sampling setup, an ultrashort pulsed electron generation system, and a THz streaking system with a simple butterfly shaped optoelectronic device. The electron pulse duration was estimated to be 2.6 ps using an extremely weak THz pulse (2.6 kV/cm) on a simple THz optoelectronic resonator. Because multiple deflections would not occur in a shorter electron pulse (<0.6 ps), the required THz intensity would be even smaller than in the present case. We cannot generate a shorter electron pulse in this setup due to the geometry of the electron source. However, we have developed ultrafast time-resolved electron diffraction setups at 75^{14,48,49} and 100 keV³⁵ accelerations with a radio frequency compression cavity. These two setups provide an electron pulse duration of ~ 1 ps or <100 fs. For future experiments, measuring shorter and longer durations of electron pulses by applying the THz streaking setup to these time-resolved electron diffractometers would be important. Comparing the convolution of a temporal profile of the electron pulse and electric field in a THz optoelectronic resonator with the Fourier components of a deflection time profile is an effective method for characterizing an electron pulse with a duration longer than a THz wave period. In the present study, the streaking signal overlaps because the electron pulse duration is longer than the half period of the main component of the THz wave. However, we can also address that, for future experiments, measurements with a higher time resolution (less than 10 fs) can be realized using the THz streaking method for time-resolved electron diffraction measurements, i.e., three beams (an optical pulse for the pump line, an electron pulse for the probe line, and a THz pulse for the streaking line) can be used for the pump–probe experiment using a short electron pulse (<0.6 ps) without multiple deflections.⁵⁰

ASSOCIATED CONTENT

Supporting Information

The Supporting Information is available free of charge at <https://pubs.acs.org/doi/10.1021/acsp Photonics.2c01304>.

Detailed description of the three-dimensional electric field at the THz resonator, RLC model of the resonator, Hilbert transform of the deflection of the electron beam, electron beam deflection in detail, and additional characterization of electron deflection by a THz wave (PDF)

AUTHOR INFORMATION

Corresponding Authors

Yusuke Arashida – Graduate School of Science and Technology, University of Tsukuba, Tsukuba 305-8573, Japan; orcid.org/0000-0001-6366-3934; Email: arashida.yusuke.kb@u.tsukuba.ac.jp

Masaki Hada – Graduate School of Science and Technology and Tsukuba Research Center for Energy Materials Science (TREMS), University of Tsukuba, Tsukuba 305-8573, Japan; orcid.org/0000-0001-8148-0971; Email: hada.masaki.fm@u.tsukuba.ac.jp

Authors

Wataru Yajima – Graduate School of Science and Technology, University of Tsukuba, Tsukuba 305-8573, Japan; orcid.org/0000-0002-8581-768X

Ryota Nishimori – College of Engineering Sciences, University of Tsukuba, Tsukuba 305-8573, Japan

Yuga Emoto – Graduate School of Science and Technology, University of Tsukuba, Tsukuba 305-8573, Japan

Yuki Yamamoto – Graduate School of Science and Technology, University of Tsukuba, Tsukuba 305-8573, Japan; orcid.org/0000-0002-4132-1236

Kohei Kawasaki – Graduate School of Science and Technology, University of Tsukuba, Tsukuba 305-8573, Japan

Yuri Saida – Graduate School of Science and Technology, University of Tsukuba, Tsukuba 305-8573, Japan; orcid.org/0000-0003-2489-1701

Samuel Jeong – Graduate School of Science and Technology, University of Tsukuba, Tsukuba 305-8573, Japan

Keishi Akada – Graduate School of Science and Technology, University of Tsukuba, Tsukuba 305-8573, Japan

Kou Takubo – School of Science, Tokyo Institute of Technology, Tokyo 152-8551, Japan; orcid.org/0000-0002-2591-1244

Hidemi Shigekawa – Graduate School of Science and Technology, University of Tsukuba, Tsukuba 305-8573, Japan; orcid.org/0000-0001-9550-5148

Jun-ichi Fujita – Graduate School of Science and Technology, University of Tsukuba, Tsukuba 305-8573, Japan

Shin-ya Koshihara – School of Science, Tokyo Institute of Technology, Tokyo 152-8551, Japan

Shoji Yoshida – Graduate School of Science and Technology, University of Tsukuba, Tsukuba 305-8573, Japan

Complete contact information is available at:

<https://pubs.acs.org/10.1021/acsp Photonics.2c01304>

Funding

This work was supported by Kakenhi Grants-in-Aid (Nos. JP18H05208, JP19H00847, and JP20H01832) and the Leading Initiative for Excellent Young Researchers of the Ministry of Education, Culture, Sports, Science and Technology (MEXT), Japan. This work was also supported by JST FOREST Program, Grant No. JPMJFR211V. A part of this work was supported by “Advanced Research Infrastructure for Materials and Nanotechnology in Japan (ARIM)” of the Ministry of Education, Culture, Sports, Science and Technology (MEXT); Grant No. JPMXP1222BA0009.

Notes

The authors declare no competing financial interest.

REFERENCES

- (1) Zewail, A. H. Femtochemistry: Atomic-Scale Dynamics of the Chemical Bond. *J. Phys. Chem. A* **2000**, *104*, 5660–5694.
- (2) Siwick, B. J.; Dwyer, J. R.; Jordan, R. E.; Miller, R. J. D. An Atomic-Level View of Melting Using Femtosecond Electron Diffraction. *Science* **2003**, *302*, 1382–1385.
- (3) Baum, P.; Yang, D.-S.; Zewail, A. H. 4D Visualization of Transitional Structures in Phase Transformations by Electron Diffraction. *Science* **2007**, *318*, 788–792.
- (4) Gao, M.; Lu, C.; Jean-Ruel, H.; Liu, L. C.; Marx, A.; Onda, K.; Koshihara, S.; Nakano, Y.; Shao, X.; Hiramatsu, T.; Saito, G.; Yamochi, H.; Cooney, R. R.; Moriena, G.; Sciaini, G.; Miller, R. J. D. Mapping Molecular Motions Leading to Charge Delocalization with Ultrabright Electrons. *Nature* **2013**, *496*, 343–346.
- (5) Miller, R. J. D. Femtosecond Crystallography with Ultrabright Electrons and X-rays: Capturing Chemistry in Action. *Science* **2014**, *343*, 1108–1116.

- (6) Morrison, V. R.; Chatelain, R. P.; Tiwari, K. L.; Hendaoui, A.; Bruhacs, A.; Chaker, M.; Siwick, B. J. A Photoinduced Metal-Like Phase of Monoclinic VO₂ Revealed by Ultrafast Electron Diffraction. *Science* **2014**, *346*, 445–448.

- (7) Ishikawa, T.; Hayes, S. A.; Keskin, S.; Corthey, G.; Hada, M.; Pichugin, K.; Marx, A.; Hirscht, J.; Shionuma, K.; Onda, K.; Okimoto, Y.; Koshihara, S.; Yamamoto, T.; Cui, H.; Nomura, M.; Oshima, Y.; Abdel-Jawad, M.; Kato, R.; Miller, R. J. D. Direct Observation of Collective Modes Coupled to Molecular Orbital-Driven Charge Transfer. *Science* **2015**, *350*, 1501–1505.

- (8) Gliserin, A.; Walbran, M.; Krausz, F.; Baum, P. Sub-Phonon-Period Compression of Electron Pulses for Atomic Diffraction. *Nat. Commun.* **2015**, *6*, 8723.

- (9) Feist, A.; Echemkamp, K. E.; Schauss, J.; Yalunin, S. V.; Schäfer, S.; Ropers, C. Quantum Coherent Optical Phase Modulation in an Ultrafast Transmission Electron Microscope. *Nature* **2015**, *521*, 200–203.

- (10) Waldecker, L.; Miller, T. A.; Rudé, M.; Bertoni, R.; Osmond, J.; Pruneri, V.; Simpson, R. E.; Ernstorfer, R.; Wall, S. Time-Domain Separation of Optical Properties from Structural Transitions in Resonantly Bonded Materials. *Nat. Mater.* **2015**, *14*, 991–995.

- (11) Morimoto, Y.; Baum, P. Diffraction and Microscopy with Attosecond Electron Pulse Trains. *Nat. Phys.* **2018**, *14*, 252–256.

- (12) Sie, E. J.; Nyby, C. M.; Pemmaraju, C. D.; Park, S. J.; Shen, X.; Yang, J.; Hoffmann, M. C.; Ofori-Okai, B. K.; Li, R.; Reid, A. H.; Weathersby, S.; Mannebach, E.; Finney, N.; Rhodes, D.; Chenet, D.; Antony, A.; Balicas, L.; Hone, J.; Devereaux, T. P.; Heinz, T. F.; Wang, X.; Lindenberg, A. M. An Ultrafast Symmetry Switch in a Weyl Semimetal. *Nature* **2019**, *565*, 61–66.

- (13) Li, Z.; Gyawali, S.; Ischenko, A. A.; Hayes, S.; Miller, R. J. D. Mapping Atomic Motions with Electrons: Toward the Quantum Limit to Imaging Chemistry. *ACS Photonics* **2020**, *7*, 296–320.

- (14) Hada, M.; Nishina, Y.; Kato, T. Exploring Structures and Dynamics of Molecular Assemblies: Ultrafast Time-Resolved Electron Diffraction Measurements. *Acc. Chem. Res.* **2021**, *54*, 731–743.

- (15) Srinivasan, R.; Lobastov, V. A.; Ruan, C.-Y.; Zewail, A. H. Ultrafast Electron Diffraction (UED) A New Development for the 4D Determination of Transient Molecular Structures. *Helv. Chim. Acta* **2003**, *86*, 1761–1799.

- (16) King, W. E.; Campbell, G. H.; Frank, A.; Reed, B.; Schmerge, J. F.; Siwick, B. J.; Stuart, B. C.; Weber, P. M. Ultrafast Electron Microscopy in Materials Science, Biology, and Chemistry. *J. Appl. Phys.* **2005**, *97*, 111101.

- (17) Miller, R. J. D.; Ernstorfer, R.; Harb, M.; Gao, M.; Hebeisen, C. T.; Jean-Ruel, H.; Lu, C.; Moriena, G.; Sciaini, G. ‘Making the Molecular Movie’: First Frames. *Acta Crystallogr., Sect. A* **2010**, *66*, 137–156.

- (18) Hada, M.; Pichugin, K.; Sciaini, G. Ultrafast Structural Dynamics with Table Top Femtosecond Hard X-ray and Electron Diffraction Setups. *Eur. Phys. J. Spec. Top.* **2013**, *222*, 1093–1123.

- (19) Manz, S.; Casandru, A.; Zhang, D.; Zhong, Y.; Loch, R. A.; Marx, A.; Hasegawa, T.; Liu, L. C.; Bayesteh, S.; Delsim-Hashemi, H.; Hoffmann, M.; Felber, M.; Hachmann, M.; Mayet, F.; Hirscht, J.; Keskin, S.; Hada, M.; Epp, S. W.; Flöttmann, K.; Miller, R. J. D. Mapping Atomic Motions with Ultrabright Electrons: Towards Fundamental Limits in Space-Time Resolution. *Faraday Discuss.* **2015**, *177*, 467–491.

- (20) Siwick, B. J.; Green, A. A.; Hebeisen, C. T.; Miller, R. J. D. Characterization of Ultrashort Electron Pulses by Electron-Laser Pulse Cross Correlation. *Opt. Lett.* **2005**, *30*, 1057–1059.

- (21) Hebeisen, C. T.; Ernstorfer, R.; Harb, M.; Dartigalongue, T.; Jordan, R. E.; Miller, R. J. D. Femtosecond Electron Pulse Characterization Using Laser Ponderomotive Scattering. *Opt. Lett.* **2006**, *31*, 3517–3519.

- (22) Gao, M.; Jean-Ruel, H.; Cooney, R. R.; Stampe, J.; de Jong, M.; Harb, M.; Sciaini, G.; Moriena, G.; Miller, R. J. D. Full Characterization of RF Compressed Femtosecond Electron Pulses

- Using Ponderomotive Scattering. *Opt. Express* **2012**, *20*, 12048–12058.
- (23) Morrison, V. R.; Chatelain, R. P.; Godbout, C.; Siwick, B. J. Direct Optical Measurements of the Evolving Spatio-Temporal Charge Density in Ultrashort Electron Pulses. *Opt. Express* **2013**, *21*, 21–29.
- (24) Gerbig, C.; Senftleben, A.; Morgenstern, S.; Sarpe, C.; Baumert, T. Spatio-Temporal Resolution Studies on a Highly Compact Ultrafast Electron Diffractometer. *New J. Phys.* **2015**, *17*, 043050.
- (25) Kassier, G. H.; Haupt, K.; Erasmus, N.; Rohwer, E. G.; Von Bergmann, H. M.; Schwoerer, H.; Coelho, S. M. M.; Auret, F. D. A Compact Streak Camera for 150 fs Time Resolved Measurement of Bright Pulses in Ultrafast Electron Diffraction. *Rev. Sci. Instrum.* **2010**, *81*, 105103.
- (26) Kassier, G. H.; Erasmus, N.; Haupt, K.; Boshoff, I.; Siegmund, R.; Coelho, S. M. M.; Schwoerer, H. Photo-Triggered Pulsed Cavity Compressor for Bright Electron Bunches in Ultrafast Electron Diffraction. *Appl. Phys. B: Laser Opt.* **2012**, *109*, 249–257.
- (27) Gao, M.; Jiang, Y.; Kassier, G. H.; Miller, R. J. D. Single Shot Time Stamping of Ultrabright Radio Frequency Compressed Electron Pulses. *Appl. Phys. Lett.* **2013**, *103*, 033503.
- (28) Fabiańska, J.; Kassier, G.; Feurer, T. Split Ring Resonator Based THz-Driven Electron Streak Camera Featuring Femtosecond Resolution. *Sci. Rep.* **2015**, *4*, 5645.
- (29) Kealhofer, C.; Schneider, W.; Ehberger, D.; Ryabov, A.; Krausz, F.; Baum, P. All-Optical Control and Metrology of Electron Pulses. *Science* **2016**, *352*, 429–433.
- (30) Zhang, D.; Fallahi, A.; Hemmer, M.; Wu, X.; Fakhari, M.; Hua, Y.; Cankaya, H.; Calendron, A.-L.; Zapata, L. E.; Matlis, N. H.; Kärtner, F. X. Segmented Terahertz Electron Accelerator and Manipulator (STEAM). *Nat. Photonics* **2018**, *12*, 336–342.
- (31) Zhao, L.; Wang, Z.; Lu, C.; Wang, R.; Hu, C.; Wang, P.; Qi, J.; Jiang, T.; Liu, S.; Ma, Z.; Qi, F.; Zhu, P.; Cheng, Y.; Shi, Z.; Shi, Y.; Song, W.; Zhu, X.; Shi, J.; Wang, Y.; Yan, L.; Zhu, L.; Xiang, D.; Zhang, J. Terahertz Streaking of Few-Femtosecond Relativistic Electron Beams. *Phys. Rev. X* **2018**, *8*, 021061.
- (32) Li, R. K.; Hoffmann, M. C.; Nanni, E. A.; Glenzer, S. H.; Kozina, M. E.; Lindenberg, A. M.; Ofori-Okai, B. K.; Reid, A. H.; Shen, X.; Weathersby, S. P.; Yang, J.; Zajac, M.; Wang, X. J. Terahertz-Based Subfemtosecond Metrology of Relativistic Electron Beams. *Phys. Rev. Accel. Beams* **2019**, *22*, 012803.
- (33) Zhang, D.; Kroh, T.; Ritzkowski, F.; Rohwer, T.; Fakhari, M.; Cankaya, H.; Calendron, A.-L.; Matlis, N. H.; Kärtner, F. X. THz-Enhanced DC Ultrafast Electron Diffractometer. *Ultrafast Science* **2021**, *2021*, 1.
- (34) Weathersby, S. P.; Brown, G.; Centurion, M.; Chase, T. F.; Coffee, R.; Corbett, J.; Eichner, J. P.; Frisch, J. C.; Fry, A. R.; Gühr, M.; Hartmann, N.; Hast, C.; Hettel, R.; Jobe, R. K.; Jongewaard, E. N.; Lewandowski, J. R.; Li, R. K.; Lindenberg, A. M.; Makasyuk, I.; May, J. E.; McCormick, D.; Nguyen, M. N.; Reid, A. H.; Shen, X.; Sokolowski-Tinten, K.; Vecchione, T.; Vetter, S. L.; Wu, J.; Yang, J.; Dürr, H. A.; Wang, X. J. Mega-Electron-Volt Ultrafast Electron Diffraction at SLAC National Accelerator Laboratory. *Rev. Sci. Instrum.* **2015**, *86*, 073702.
- (35) Takubo, K.; Banu, S.; Jin, S.; Kaneko, M.; Yajima, W.; Kuwahara, M.; Hayashi, Y.; Ishikawa, T.; Okimoto, Y.; Hada, M.; Koshihara, S. Generation of Sub-100 Fs Electron Pulses for Time-Resolved Electron Diffraction Using a Direct Synchronization Method. *Rev. Sci. Instrum.* **2022**, *93*, 053005.
- (36) Epp, S. W.; Hada, M.; Zhong, Y.; Kumagai, Y.; Motomura, K.; Mizote, S.; Ono, T.; Owada, S.; Axford, D.; Bakhtiarzadeh, S.; Fukuzawa, H.; Hayashi, Y.; Katayama, T.; Marx, A.; Müller-Werkmeister, H. M.; Owen, R. L.; Sherrell, D. A.; Tono, K.; Ueda, K.; Westermeier, F.; Miller, R. J. D. Time Zero Determination for FEL Pump-Probe Studies Based on Ultrafast Melting of Bismuth. *Struct. Dyn.* **2017**, *4*, 054308.
- (37) Baek, I. H.; Kim, H. W.; Bark, H. S.; Jang, K.-H.; Park, S.; Shin, J.; Kim, Y. C.; Kim, M.; Oang, K. Y.; Lee, K.; Rotermund, F.; Vinokurov, N. A.; Jeong, Y. U. Real-Time Ultrafast Oscilloscope with a Relativistic Electron Bunch Train. *Nat. Commun.* **2021**, *12*, 6851.
- (38) Zhao, L.; Wang, Z.; Tang, H.; Wang, R.; Cheng, Y.; Lu, C.; Jiang, T.; Zhu, P.; Hu, L.; Song, W.; Wang, H.; Qiu, J.; Kostin, R.; Jing, C.; Antipov, S.; Wang, P.; Qi, J.; Cheng, Y.; Xiang, D.; Zhang, J. Terahertz Oscilloscope for Recording Time Information of Ultra-short Electron Beams. *Phys. Rev. Lett.* **2019**, *122*, 144801.
- (39) Frühling, U.; Wieland, M.; Gensch, M.; Gebert, T.; Schütte, B.; Krikunova, M.; Kalms, R.; Budzyn, F.; Grimm, O.; Rossbach, J.; Plönjes, E.; Drescher, M. Single-Shot Terahertz-Field-Driven X-Ray Streak Camera. *Nat. Photonics* **2009**, *3*, 523–528.
- (40) Ivanov, R.; Liu, J.; Brenner, G.; Brachmanski, M.; Düsterer, S. FLASH Free-Electron Laser Single-Shot Temporal Diagnostic: Terahertz-Field-Driven Streaking. *J. Synchrotron Radiat.* **2018**, *25*, 26–31.
- (41) Blachucki, W.; Wach, A.; Czapla-Masztafiak, J.; Delcey, M.; Arrell, C.; Fanselow, R.; Juranic, P.; Lundberg, M.; Milne, C.; Sá, J.; Szlachetko, J. Approaching the Attosecond Frontier of Dynamics in Matter with the Concept of X-ray Chronoscopy. *Appl. Sci.* **2022**, *12*, 1721.
- (42) Park, S. T.; Lin, M.; Zewail, A. H. Photon-Induced Near-Field Electron Microscopy (PINEM): Theoretical and Experimental. *New J. Phys.* **2010**, *12*, 123028.
- (43) Fülöp, J. A.; Pálfalvi, L.; Almási, G.; Hebling, J. Design of High-Energy Terahertz Sources Based on Optical Rectification. *Opt. Express* **2010**, *18*, 12311–12327.
- (44) Hirori, H.; Doi, A.; Blanchard, F.; Tanaka, K. Single-Cycle Terahertz Pulses with Amplitudes Exceeding 1 MV/cm Generated by Optical Rectification in LiNbO₃. *Appl. Phys. Lett.* **2011**, *98*, 091106.
- (45) Matsunaga, R.; Tsuji, N.; Fujita, H.; Sugioka, A.; Makise, K.; Uzawa, Y.; Terai, H.; Wang, Z.; Aoki, H.; Shimano, R. Light-Induced Collective Pseudospin Precession Resonating with Higgs Mode in a Superconductor. *Science* **2014**, *345*, 1145–1149.
- (46) Winnewisser, C.; Jepsen, P. U.; Schall, M.; Schyja, V.; Helm, H. Electro-optic detection of THz radiation in LiTaO₃, LiNbO₃ and ZnTe. *Appl. Phys. Lett.* **1997**, *70*, 3069–3071.
- (47) Ehberger, D.; Kealhofer, C.; Baum, P. Electron Energy Analysis by Phase-Space Shaping with THz Field Cycles. *Struct. Dyn.* **2018**, *5*, 044303.
- (48) Hada, M.; Norimatsu, K.; Tanaka, S.; Keskin, S.; Tsuruta, T.; Igarashi, K.; Ishikawa, T.; Kayanuma, Y.; Miller, R. J. D.; Onda, K.; Sasagawa, T.; Koshihara, S.; Nakamura, K. G. Bandgap Modulation in Photoexcited Topological Insulator Bi₂Te₃ via Atomic Displacements. *J. Chem. Phys.* **2016**, *145*, 024504.
- (49) Hada, M.; Yamaguchi, D.; Ishikawa, T.; Sawa, T.; Tsuruta, K.; Ishikawa, K.; Koshihara, S.; Hayashi, Y.; Kato, T. Ultrafast Isomerization-Induced Cooperative Motions to Higher Molecular Orientation in Smectic Liquid-Crystalline Azobenzene Molecules. *Nat. Commun.* **2019**, *10*, 4159.
- (50) Badali, D. S.; Miller, R. J. D. Robust Reconstruction of Time-Resolved Diffraction from Ultrafast Streak Cameras. *Struct. Dyn.* **2017**, *4*, 054302.